1 **Estimate of Greenland and Antarctic ice-sheet total discharge**

2 **from multiple GRACE solutions**

3 Ida Russo[1], Guillaume Ramillien[2], Frédéric Frappart[2] and Frédérique Rémy[2]

5 [1]Centro Euro-Mediterraneo per i Cambiamenti Climatici, Bologna, Italy

6 [2]LEGOS, Observatoire Midi-Pyrénées, Toulouse, France

7 *Corresponding author address:* Dr. Ida Russo, Salita Moiariello 68 – 80131 Naples, Italy.

8 *Email:* ida.russo@email.it

9 **Abstract**

10 In this work a method for the estimation of 2003-2010 monthly-mean total discharge from

11 Greenland and Antarctica is presented. We show that measurements of time-variable gravity

12 from GRACE when combined with estimates of precipitation and sublimation can

13 realistically reconstruct the total discharge from the ice-sheets into the ocean. In particular, the

14 total discharge has been calculated as a 8-member ensemble-mean obtained by combining

15 multiple GRACE solutions with water fluxes from both an high resolution regional

16 atmospheric climate model (RACMO2) and a global reanalysis (ERA-Interim). The

17 gravimetric measurements of mass variations and the precipitation and sublimation

18 atmospheric fields have been combined in the ice-sheets water mass balance equation,

19 according to the main drainage basin systems. The use of the combined land-atmosphere

20 water mass balance has also been tested, which however led to a large underestimation of

21 total discharge. A comparison among the different GRACE solutions is also performed,

22 highlighting similarities and differences and analyzing the possible causes. GRACE datasets

23 show similar ice-sheet mass trends on Antarctica and over the majority of the Greenland

24 basins, while significant differences (up to a factor of 1.9) have been found in mass-loss areas

25 characterized by strongly negative water height trends. This is likely primarily caused by the

26    different pre-processing techniques applied to the raw gravimetric data.

## 1- Introduction.

28 Freshwater inputs to the ocean from land-ice and terrestrial water storage changes

29 represent, along with the thermal expansion of sea waters, the major cause of global sea level

30 change on short time-scales (IPCC AR5, 2014).

31 Antarctica and Greenland ice-sheets represent the vast majority of the Earth's ice.

32 Satellite-based observations and SMB (surface mass balance) model simulations show a rapid

33 acceleration of ice discharge from Greenland and Antarctica ice-sheets since 1992, by

34 contributing of about 0.6 mm/yr to the rate of global sea level rise (Shepherd et al., 2012). The

35 increasing ice mass loss from the polar ice-sheets is in particular due to an acceleration of

36 flow speed of large West Antarctica outlet glaciers system (IMBIE team, 2018) and to an

37 increase in runoff from the surface water melting in Greenland (Enderlin et al., 2014).

38 Furthermore, recent observations suggest that ice dynamics may be a key factor in the

39 response of coastal glaciers and ice-sheets melting especially in West Antarctica (Flament and

40 Rémy, 2012). In Greenland, laser altimetric observations indicate a thickening of the high

41 central ice-sheet during the 2003-2007 period, but also a significant increased loss from

42 coastal outlet glaciers, due to surface melting and accelerated flow, has occurred (Zwally et

43 al., 2011). Ice thickness surveys by NASA's Operation IceBridge suggest that, since 2009,

44 surface mass balance rather than ice dynamics has dominated Greenland contribution to sea

45 level rise (Enderlin et al., 2014). The Antarctic ice-sheet system is more complex, and

46 presents large regional differences. Ice loss in West Antarctica is mostly due to the

47 acceleration of outlet glaciers and, as a secondary effect, to enhanced melting caused by

48 increasing temperature. In contrast, surface temperatures over most of East Antarctica are

49 well below the freezing point and a small increase in air temperature cannot initiate melt

50 (Stoddart et al., 2008). The cause of acceleration of other large outlet glaciers in West

51    Antarctica is not fully understood, but may be related to sea-ice shelf instability (Holland et

52    al., 2008; Mouginot et al., 2014). In terms of equivalent sea level rise, Greenland and

53    Antarctica contributions have been estimated to be 0.17 mm/yr during the period 1992-2001

54    and 1.0 mm/yr during 2002-2011, which means that a six-fold increase in mass loss compared

55    to 1992-2001 period occurred during the recent period (IPCC AR5, 2014). Furthermore,

56    empirical methods based on the extrapolation of the ice-sheets induced sea level rise from

57    Atmosphere Ocean General Circulation Models (AOGCMs) projections, suggest that such a

58    contribution will be increasingly positive in the future (Gregory and Huybrechts, 2006).

59        Due to the increasing contribution of ice-sheets melting into the ocean and their important

60    positive contribution to sea level variations, the availability of realistic estimates of ice-sheet

61    total discharge is of major importance for the investigation and monitoring of sea level rise

62    and to understand how the Earth system is responding to anthropogenic-induced global

63    warming. If there exists no comprehensive global network for the monitoring of freshwater

64    discharge into the world oceans (Alsdorf and Lettenmaier, 2003; Brakenridge et al., 2005), the

65    situation is even worse for the Greenland and Antarctica ice sheets. Over land, river

66    discharges are unevenly distributed, discontinuous over time, and have variable accuracies. To

67    provide reliable estimates of river discharges, Fekete et al. (2000, 2002) followed a data-

68    merging approach by using observed discharge data from the Global Runoff Data Center

69    (GRDC; http://grdc.bafg.de) to constrain modeled estimates of runoff. Later, Dai and

70    Trenberth (2002) improved the previous work by incorporating a river-routing scheme for the

71    appropriate transport of the runoff into the ocean. Alternatively, terrestrial water storage

72    (TWS) observations from GRACE satellite gravimetry mission combined with precipitation

73    and evaporation data have been used to solve the water balance equation at basin-scale (or

74    similarly estimating precipitation and evaporation using the atmospheric water balance

75    equation) for the terrestrial freshwater discharge (Syed et al., 2007; Syed et al., 2009). In this

76    study we present a new strategy for the calculation of an ensemble of monthly ice-sheet total

77    discharge estimates, which, in the comparison with observations, has proved to be the best

78    solution to reproduce realistic estimates of Greenland and Antarctica freshwater input into the

79    ocean. According to the main drainage basin systems of the ice-sheet, we have constructed a

80    2003-2010 interannual dataset of total discharge from Greenland and Antarctica, calculated

81    by combining GRACE gravimetry observations of ice-sheets mass loss and atmospheric

82    model data of precipitation and sublimation. Differently from previous works, this is the first

83    time that such a calculation is made over the ice-sheets regions, highlighting the innovation of

84    the present study. Furthermore, multiple GRACE solutions and two different datasets of

85    atmospheric model outputs have been applied in the calculation of the total discharge

86    estimates. The importance of this study also resides in the potential application of such a

87    dataset in the frame of ocean modelling. In fact, due to the lack of time-varying runoff

88    measurements, land and ice runoff used in the current OGCMs simulations consist of

89    climatological estimates that are assumed not to vary inter-annually; the increasing freshwater

90    input from ice-sheets into the ocean is thus not considered in ocean simulations.

91       This study is structured as follows: we firstly introduce the methods (Section 2) and

92    datasets used for the total discharge calculation (Section 3); in Section 4 we show the

93    comparison among the different GRACE solutions; in Section 5 we present the results of the

94    total discharge calculation and in Section 6 the use of different precipitation datasets to

95    calculated the ice-sheet total discharge is performed and discussed; in Section 7 the main

96    conclusions are summarized followed by a discussion.

97

98

## 2- Approaches to compute total discharge from the ice-sheets.

99

100    Ice-sheet total discharge from Greenland and Antarctica were estimated by using two

101    approaches, namely through the application of the land water mass balance equation (Syed et

102    al., 2010) and the atmospheric water mass balance equation (Syed et al., 2009) over land (i.e.,

103    large river basins, drainage regions and continents). Here, we use a similar approach which is

104    described in detail below.

105

106

107    **2.1- Resolution of the surface mass balance.**

108    In the first approach, the total discharge is calculated using the ice-sheets water mass

109    balance equation:

110    $$\frac{\partial M}{\partial t} = SMB - D \qquad (1)$$

111

112    where $\frac{\partial M}{\partial t}$ is the variation of mass in time over the ice-sheet; SMB = P – E - R is the

113    surface mass balance, equal to the sum of solid and liquid precipitation (P), evaporation and

114    sublimation (E) and meltwater runoff (R, note that this term is negligible in Antarctica where

115    total discharge is almost totally due to ice flow; Van den Broeke et al., 2011); D is the ice

116    discharge, i.e. the iceberg calving, that is the main process through which Antarctica ice-sheet

117    is losing mass. The estimate of the total discharge (i.e. the sum of meltwater runoff R and

118    solid ice discharge D) leaving the ice-sheet is therefore equal to:

119    $$R + D = P - E - \frac{\partial M}{\partial t} \qquad (2)$$

120

121     The balance was applied to the whole of Greenland and Antarctica ice-sheets according to

122     their main drainage basin systems, by computing the total volume of M, P and E within every

123     $k$ drainage basins (Eq. (3), (4) and (5) ):

124     $$V_M^k(t) = \sum M(\lambda_{ij}, \theta_{ij}, t) * \cos\theta_{ij} * d\lambda_{ij} * d\theta_{ij} \tag{3}$$

125     $$V_P^k(t) = \sum P(\lambda_{ij}, \theta_{ij}, t) * \cos\theta_{ij} * d\lambda_{ij} * d\theta_{ij} \tag{4}$$

126     $$V_E^k(t) = \sum E(\lambda_{ij}, \theta_{ij}, t) * \cos\theta_{ij} * d\lambda_{ij} * d\theta_{ij} \tag{5}$$

127

128     where $\theta$ and $\lambda$ are latitude and longitude, respectively.

129     Geographical masks of the ice-sheets drainage system regions, based on surface slopes

130     analyses, were derived from Luthcke et al. (2006) for Greenland and based on the sub-

131     division of Rignot et al. (2008) for Antarctica. Greenland was thereby divided into 6 drainage

132     basins (Figure 1) and Antarctica into 18.

133     Since GRACE data are given as monthly anomalies of mass, water storage changes are

134     considered to have occurred between the mid-point (i.e. the 15th day) of two consecutive

135     months. We have therefore computed compatible estimates of P and E by integrating daily

136     averages between the 15th day of consecutive months as follows:

137     $$\int V_{R+D}^k \, dt = \int V_{P-E}^k \, dt - \left[ \left( V_M^k \right)_{m+1} - \left( V_M^k \right)_m \right] \tag{6}$$

138

139     where $\left( V_M^k \right)_m$ is the total volume of M over a certain drainage basin of Greenland/Antarctica

140     expressed in equivalent water mass anomaly of the month $m$. This procedure was possible

141     only for daily ERA-Interim data since RACMO data were available as monthly means only.

142

143

### 2.2- The land-atmosphere mass balance.

144

145    In the second approach, the ice-sheet total discharge is computed by the use of the

146    combined land-atmosphere water mass balance equation, obtained from Eq. (1) and the

147    atmospheric moisture budget expressed as:

148
$$\frac{\partial W}{\partial t} = E - P - \nabla \vec{Q} \qquad (7)$$

149    where W is the total column water vapor and the last term on the right hand side is the

150    horizontal divergence of the vertically integrated vapor flux.

151    By combining Eq. (1) and (7) we therefore obtain the total discharge (R+D) now

152    expressed as:

153
$$R + D = -\frac{\partial M}{\partial t} - \frac{\partial W}{\partial t} - \nabla \vec{Q} \qquad (8)$$

154

155    On land, the method of Eq. (8) has been proved more accurate than Eq. (2) due to the large

156    uncertainty in the atmospheric models evapotranspiration that is bypassed by the use of the

157    combined land-atmosphere water mass balance equation (Syed et al. 2009). This is however

158    questionable on land-ice, where the contribution of evaporation is negligible and large

159    uncertainties on atmospheric moisture remain due to lack of a proper observational network.

160    Finally, the use of 8-member ensemble-mean total discharge has been tested. The

161    ensemble-mean solution has been calculated by averaging the eight $R+D$ fields, obtained

162    from Eq. (2), calculated by balancing, in turn, each of the four GRACE EWH dataset (JPL,

163    CSR, GFZ and GRGS) once with RACMO2 regional model data and once with ERA-Interim

164    atmospheric fields of precipitation and sublimation; these results will be discussed in detail in

165    Section 5.

166

167

**3- Datasets.**

**3.1- GRACE solutions for water mass variations.**

The GRACE space mission, sponsored by National Aeronautics and Space Administration (NASA) and Deutsches Zentrum fur Luft- und Raumfahrt (DLR), has been collecting gravity variations measurements since March 2002. It provides, at regular time intervals, monthly and 10-day global solutions of the Earth gravity field (e.g. Wahr et al., 1998; Tapley et al., 2004; Schmidt et al., 2006). These solutions are provided by different official centers as lists of Stokes coefficients (i.e., spherical harmonic coefficients of the geo-potential) up to degree 50-60, or equivalently at spatial resolution of 300-400 km. Changes in the gravity field are largely caused by the redistribution of water mass in the hydrological cycle (Wahr et al., 1998, 2004). GRACE measurements have enabled for the very first time to derive satellite-based global maps of terrestrial water storage variations. The Stokes coefficients are converted into surface mass density and expressed in units of mm of equivalent water height (Ramillien et al., 2006b). The solutions will be later called "equivalent water height differences" (EWH) since they are expressed as differences between the time-variable solution and a mean static gravity field.

In the present work we have tested the use of multiple GRACE solutions, released by different research groups: Deutsches Geo Forschungs Zentrum (GFZ - Potsdam, Germany), NASA Jet Propulsion Laboratory (JPL - US), Center for Space Research (CSR - US) and Groupe de Recherche de Géodésie Spatiale (GRGS) at the Center National d'Etudes Spatiales (CNES - Toulouse, France). These are monthly solutions at 330 km of spatial resolution (i.e. up to degree 60 of the spherical harmonics). Different pre-processing methods have been used

190 to low-pass filter the high frequencies of the noise contained in the GRACE solutions.

191 Moreover, applying an Independent Component Analysis (ICA) enabled us to separate water

192 mass variations, which are meaningful geophysical signals, from the polluting noise, in

193 particular the North-South striping. This post-processing technique was only applied to the

194 CSR, GFZ and JPL data, which will be called "ICA-based" solutions in order to distinguish

195 them from the GRGS data. In this paper, the more recent releases have been used for both the

196 solutions: RL05 for ICA and RL03 for GRGS solution.

197 Once averaged over large geographical areas, the accuracy of the GRACE-estimated water

198 mass change should not exceed 1.5 cm of equivalent-water height (Wahr et al., 2004;

199 Ramillien et al, 2006a). Total errors in the Stokes coefficients are a combination of

200 instrumental and processing uncertainties, effects of the truncation of the spherical harmonic

201 spectrum (i.e., omission and leakage errors) and the lack of completeness of the dealiasing

202 models used to remove the gravitational effects of varying atmospheric and oceanic masses

203 (Velicogna and Wahr, 2013).

204 To have an idea of the mass variations of the two ice-sheets, we present the linear trends

205 (over the period 2003-2012) of EWH for the CSR solution (Figure 2). We can observe a

206 strong decrease of mass over West Antarctica (more than 10 cm/yr of equivalent water height)

207 and a slight decreasing trend over the Antarctic Peninsula. East Antarctica shows neither loss

208 nor accumulation of mass. Most of the Greenland ice-sheet is characterized by ice mass loss

209 mostly concentrated in the south-eastern part but also on the northern-west edge of the ice-

210 sheet, for the considered time frame.

211 As GRACE also detects multi-year deformation of the Earth surface such as the constant

212 Post Glacial Rebound (PGR) re-adjustment of the last deglaciation, we have to remove this

213 effect in our mass balance estimates. For this purpose, we used the global ICE-5G ice de-

214    glaciation model (Peltier, 2004; Paulson et al., 2007) to estimate the PGR trends over

215    Antarctica and Greenland. While the PGR effect is negligible for the Greenland ice-sheet, it is

216    significant on Antarctica where the PGR rate can be of the same order of magnitude as the

217    long-term ice mass change. Unfortunately, as PGR effects cannot be modelled accurately,

218    uncertainties in our PGR-related trends, and consequently on our mass balance estimates, are

219    suspected over Antarctica where the geological and long-term GPS observations that are used

220    in the PGR simulation remain rare (Peltier, 2009).

221

222

223    **3.2- Precipitation and evaporation data.**

224         For precipitation and sublimation (terms P and E in Eq. (2) ), we considered two different

225    datasets: ERA-Interim atmospheric reanalyses and outputs from a regional atmospheric

226    climate model. Furthermore, we have tested the use of other datasets of precipitation in the

227    estimation of $R+D$ derived from ice-sheet water mass balance and thus compared the results;

228    these additional precipitation datasets are: CMAP, GPCP and Sheffield data.

229         ERA-Interim is third generation global atmospheric reanalysis produced by the European

230    Center for Medium-range Weather Forecasts (ECMWF). ERA-Interim covers the period from

231    1 January 1979 onwards, and continues to be extended forward in near-real time. Gridded

232    data products include a large variety of 3-hourly surface parameters, describing weather as

233    well as ocean-wave and land-surface conditions, and 6-hourly upper-air parameters covering

234    the troposphere and stratosphere. Vertical integrals of atmospheric fluxes and other derived

235    fields have also been produced (Simmons et al., 2007; Dee et al., 2011). In our work we have

236    used daily precipitation and sublimation fields at a horizontal resolution of 0.75°.

237    Furthermore, we have applied a Gaussian filter with 400 km radius, in order to be consistent

238    with the spatial resolution of GRACE data.

239        In this study we used the monthly outputs of 22-year simulations (1989-2010) performed

240    with the Regional Atmospheric Climate Model (RACMO2) at high horizontal resolution of 11

241    km over Greenland and 55 km over Antarctica (van Meijgaard et al., 2008; Ettema et al.,

242    2009). The model has been developed since 2005 at Koninklijk Nederlands Meteorologisch

243    Instituut (KNMI) and is the second version of the regional climate model RACMO. This new

244    version was built on the ECMWF physics package from cycle 23r4 embedded in the semi-

245    Lagrangian (sL) dynamics kernel of the Numerical Weather Prediction (NWP) model

246    HIRLAM5.0.6 (Undén et al., 2002). The model has been forced at the lateral boundaries and

247    at the sea surface by ERA-Interim atmospheric fluxes from ECMWF operational analyses.

248    The RACMO2 outputs consist of SMB, total precipitation and runoff fields. The sublimation

249    fields have been deduced through the simple relation SMB = P - E – R . Nevertheless, the

250    sublimation is not large and not very variable and the total precipitation and runoff determine

251    most of the variability.

252        Regarding the total column water vapor and the horizontal divergence of the vertically

253    integrated vapor flux, required for the coupled land–atmosphere water balance of equation (4)

254    we used only ERA-Interim data product, as these parameters are not available from RACMO.

255

256

257    **4- Comparison of GRACE solutions.**

258        In Figure 3 the comparison between the time series of equivalent water height difference

259    among all the GRACE solutions, over Greenland, East and West Antarctica, is shown. EWH

260    time series of Figure 3 show that East Antarctica is experiencing an increasing of mass, with

261    an acceleration since 2009. In contrast, West Antarctica and Greenland are losing mass since

262   2003. The former shows a mass loss acceleration developing in August 2007, while the latter

263   shows a pronounced negative trend through the whole time-span. The four GRACE datasets

264   show similar ice-sheet mass trend on Antarctica and over the whole Greenland ice-sheet. To

265   deepen our analysis, we have compared EWH time-series for the different Greenland drainage

266   basins (Figure 4), evidencing the south-east Greenland coast (*basin 4*) as the area of highest

267   mass loss of the ice-sheet, while the total discharge flux reaches its minimum values in

268   correspondence of the north-eastern edge (*basin 2*). Even if in agreement in terms of

269   maximum and minimum areas of mass change, the two groups of GRACE solutions, GRGS

270   and ICA-based solutions, show significant differences in terms of trend magnitude. The major

271   difference has been found at northern-west Greenland (*basin 1*, Figure 5 top panel), where the

272   GRGS solution present a trend almost twice higher than the ICA one, which means a

273   considerable impact in terms of equivalent sea level contribution from Greenland ice-sheet.

274   Significant differences are also evident at the eastern coast, where the EWH trend of the two

275   groups of solutions differ by a factor of 1.5 (*basin 3*) and 1.1 (*basin 2*). The difference is even

276   more amplified in the southern-east part (*basin 4*), i.e. the area of highest ice mass loss. Over

277   this particular drainage basin, the GRGS EWH time series exhibit an ice mass loss rates 1.6

278   times higher than JPL: -15.48 cm/yr with respect to -9.51 cm/yr (Figure 5, bottom panel).

279       Several causes can give rise to the marked differences in equivalent water height trends of

280   the two groups of solutions. A considerable part is attributable to the different pre- and post-

281   processing techniques applied to the two different GRACE datasets. In fact, distinct pre-

282   processing methods have been used to filter out the high frequencies from the noisy GRACE

283   solutions, in order to extract realistic hydrological signals on the continents. In particular,

284   stabilization method have been applied to Level-1 of GRGS solutions and a Gaussian filter

285   have been applied to Level-2 of CSR, GFZ, JPL solutions. The reader is referred to Wahr et

286    al. (1998) for further details on GRACE data processing. A secondary effect of Gaussian filter

287    method is to cut off the high frequencies from the EWH signal, which are then redistributed

288    and spread over the surrounding areas. In fact, if the trend computation is not limited to the

289    Greenland ice-sheet land but extended over a bigger area which also includes the surrounding

290    ocean, few degrees off Greenland coasts, we can see a better match between GRGS and ICA

291    datasets trend (Figure 6). In this case, in fact, the high frequencies, cut off by Gaussian filter

292    method and redistributed in the surrounding areas, are now included in the ICA solutions

293    trend, which now differ from GRGS by a factor of 1.4 and 1.2 for *basin 1* and *basin 4*,

294    respectively. An additional effect that further influences *basin 1* is the positive EWH trend

295    over Canada and the Canadian Arctic Archipelago, which is distinctively visible before the

296    PGR correction (see Figure 2). This effect is probably spread over the close North-West

297    Greenland with the consequence of further decreasing the negative ICA solution trend with

298    respect to the GRGS one. Another possible source of difference is the application of the ICA

299    method, employed to further filter the CSR, GFZ and JPL solutions, which has not been

300    applied to the GRGS solution. In particular, this post-processing technique has been used with

301    the aim to reduce the presence of north-south striping due to orbit resonance that limits the

302    geophysical interpretation of the signal (Frappart et al., 2010, 2011). In order to test this

303    hypothesis a comparison among EWH time-series before and after the application of the ICA

304    method has been performed (not shown). Results suggest that the application of the ICA

305    method is not responsible for the differences in EWH trends of the two groups, conversely

306    after the application of this post-processing technique, EWH time-series of the ICA-based

307    solution result to be closer to the GRGS solution tendency (not shown). Moreover, other

308    possible causes can be attributed to differences in the static gravity field removed to the time-

309    varying solution and to differences in the oceanic/atmospheric models used to dealias the

310  GRACE solutions in order to remove the atmospheric pressure influence on satellite orbits

311  and on the ocean state.

312

313

### 5- Total discharge results.

315      In order to validate the total discharge estimates from Greenland and Antarctica and hence

316  to assess our method as a proper strategy for the realistic reconstruction of $R+D$, we have

317  compared the results obtained from Eq. (2) and (8) with measurements of ice discharge,

318  obtained by combining maps of surface velocities along ice-sheet coasts from InSAR data and

319  ice thickness from Digital Elevation Model (DEM, Rignot et al., 2011). The comparison is

320  made by subtracting the meltwater runoff (R) from the total discharge $R+D$ in order to have

321  consistent data with InSAR observations. Note that in the case of Antarctica a direct

322  comparison is allowed, since runoff from the surface water melting is a negligible process at

323  those latitudes and mass loss happens thus almost exclusively through solid ice discharge

324  (Van den Broeke et al., 2011).

325      Results are displayed in Figure 7. Here we present the ice-discharge estimates obtained by

326  using CSR GRACE data balanced once with RACMO (green line) and once with ERA-

327  Interim (cyan line) precipitation and sublimation fields. Both estimates have been calculated

328  by means of the ice-sheets water mass balance equation (2). In the comparison (Figure 7), we

329  found that the use of precipitation and sublimation fields from RACMO regional model

330  (green line) slightly overestimates observation values (magenta line) while the use of ERA-

331  Interim (cyan line) slightly underestimates them. On the other hand, the ice discharge

332  obtained by using the combined land-atmosphere water mass balance equation (8) (blue line)

333  strongly underestimates InSAR data. In light of these results, we have decided to combine the

334 two atmospheric datasets in an ensemble-mean, by also including all the GRACE solutions.

335 The 8-member ensemble-mean solution (red line) turns out to be the curve that better fits with

336 ice discharge observations; in fact, the ensemble-mean closely follows InSAR curve, except

337 for some seasonal peaks not represented by observations. At this regard, we want to underline

338 that InSAR data are available as yearly means only and this is also the reason why they cannot

339 be used for $R+D$ estimation.

340     As a further verification of the reliability of our method, in Figure 8 we have verified the

341 correct representation of the climatological seasonal cycles of Greenland and Antarctica

342 ensemble-mean total discharge. In Antarctica (bottom panel, red line) the total discharge

343 shows two minimum in November and January, in accordance with the seasonal minimum of

344 precipitation (see Figure 9 bottom panel). Precipitation over Antarctica is more abundant from

345 March to October, which is particularly evident in the RACMO2 dataset (Figure 9 bottom

346 panel, green line). In accordance, Antarctica $R+D$ starts to increases in April reaching its

347 maximum values in June after the precipitation peak. Our results are in accordance with the

348 work of Ligtenberg et al. (2012) which using a combination of a firn densification model and

349 a regional atmospheric climate model have shown that high temperatures and low

350 accumulation cause Antarctica ice-sheet surface to low in austral summer, while in autumn,

351 winter and spring the surface steadily rises, mainly due to higher accumulation rates. It is also

352 in good accordance with seasonal change of Antarctica ice-sheet height derived from

353 altimetry (Rémy et al., 2014).

354     Also over Greenland the seasonal cycle is correctly reproduced by the ensemble-mean

355 total discharge (Figure 8 top panel, red line); the summer peak is in accordance with both

356 realistic freshwater fluxes averaged over the 1991-2000 period (Marsh et al., 2010), even if

357 shifted from June to July, and different SMB models inter-comparison (Vernon et al., 2013).

358    With this further analysis we have demonstrated that our estimated $R+D$ is representative of

359    the interannual variability of the freshwater flux from land to ocean.

360

361

362    **6- Total discharge derived from ice-sheets water mass balance with different**

363    **precipitation datasets.**

364        In this study we have chosen to perform the calculation of the ice-sheet total discharge by

365    using two datasets of precipitation: ERA-Interim and RACMO2. This choice has been made

366    in order to exploit the accurateness that a third generation reanalysis, as ERA-Interim, and

367    that the high spatial resolution of a regional atmospheric model, as RACMO2, has in itself.

368    Nevertheless, several accurate precipitation products are available. We have, hence, tested the

369    use of other datasets of precipitation in the estimation of $R+D$ derived from ice-sheet water

370    mass balance and thus compared the results. In this way, we are able to assess the robustness

371    of our method, once verified the similarity among all the resulting precipitation-derived total

372    discharge.

373        The precipitation datasets involved in the comparison are CMAP, GPCP and Sheffield

374    data. The CPC Merged Analysis of Precipitation (CMAP) is a technique which produces

375    pentad and monthly analyses of global precipitation in which observations from rain gauges

376    are merged with precipitation estimates from several satellite-based algorithms (infrared and

377    microwave). The analyses are on a 2.5° x 2.5° degree latitude/longitude grid and extend back

378    to 1979 (Xie and Arkin, 1997).

379        The Global Precipitation Climatology Project (GPCP) was established by the World

380    Climate Research Program to quantify the distribution of precipitation around the globe over

381    many years. The precipitation product is obtained by optimally merging estimates computed

382   from microwave, infrared, and sounder data observed by the international constellation of

383   precipitation-related satellites, and precipitation gauge analyses. The product is available

384   since 1979 with horizontal resolution of 2.5° x 2.5° (Adler et al., 2003).

385       The Sheffield dataset of precipitation (Sheffield et al., 2006) is a global, 60-yr (1948-

386   2008), 3-hourly, 1.0° dataset of land surface hydrology fields. The dataset is constructed by

387   combining a suite of global observation-based datasets (GPCP, TRMM, GSWP-2) with the

388   National Centers for Environmental Prediction–National Center for Atmospheric Research

389   (NCEP–NCAR) reanalysis.

390       In Figure 8, we compare mean seasonal ice-sheet total discharge derived with the mass

391   balance equation (Eq. 2) by using different precipitation datasets: ERA-Interim (cyan line),

392   RACMO (green line), CMAP (black line), GPCP (orange line) and Sheffield (magenta line).

393   The comparison among the precipitation products is also shown (Figure 9). We can see that

394   the various estimated $R+D$ are of the same order of magnitude on both Greenland (top) and

395   Antarctica (bottom), with RACMO and Sheffield presenting the highest values of

396   precipitation (Figure 9) and hence of total discharge values (Figure 8). Also in terms of

397   seasonal cycle, all the precipitation-derived $R+D$ show a strongly similar interannual

398   variability, presenting the same summer peaks of discharge in June and July. The similar

399   behavior detected, confirms the robustness of our method and the reliability of the

400   precipitation data, ERA-Interim and RACMO2, used in our study. It is however worthy to

401   underline that caution has to be taken when precipitation reanalyses data are used for a study

402   of Antarctica mass balance (Bromwich et al., 2011). In fact, data assimilation is still

403   challenging in this region as reanalyses rely heavily upon a small number of ground-based

404   and upper-air observations in Antarctica, especially in the interior of the ice-sheet. Moreover,

405   the wind-blown snow (or wind-driven ablation), which, on short spatial scale, greatly affects

406   the surface mass balance over Antarctica due to the presence of katabatic winds (Rémy and

407   Frezzotti, 2006), is an important process that is not taken into account in ERA-Interim

408   reanalysis.

409

410

411   **7- Conclusions.**

412       In this study, we have proposed a strategy useful for creating an ice-sheet total discharge

413   dataset by combining multiple GRACE gravimetric data of ice mass variation on land-ice

414   with atmospheric model data of precipitation and sublimation. For the atmospheric fields, we

415   have tested the use of data from both an high resolution regional model, RACMO2, and ERA-

416   Interim reanalysis. We have demonstrated the ability of our methodology to correctly

417   reproduce realistic estimates of ice-sheet total discharge for the 2003-2010 period. In

418   particular, in the comparison with InSAR satellite observations of ice discharge, it turned out

419   that the best fit with observations is achieved with an ensemble-mean of multiple GRACE

420   solutions (JPL, CSR, GFZ and GRGS data) in combination with the two atmospheric model

421   datasets. Total discharge has been computed with the ice-sheets water mass balance equation,

422   which was applied to the main drainage basins of Greenland and Antarctica, and this is the

423   first time that such a balance is applied on land-ice. We have also tested the use of the

424   combined land-atmosphere water mass balance equation, which, however, led to a large

425   underestimation of the total discharge and has not been considered further.

426       The two groups of GRACE solutions (GRGS and ICA-based solutions) show important

427   differences in the ice mass loss 2003-2012 estimates for the southeast Greenland coast and for

428   the northwestern edge of the ice-sheet, both characterized by a strong negative signal of water

429   height trend. Namely, the GRGS solutions exhibits a faster mass loss rate with respect to the

430  ICA-based, reaching a factor of 1.9 between the GRGS (-6.01 cm/yr) and the JPL (-3.22

431  cm/yr) solution over *basin 1*. The difference in the equivalent water height trends can be

432  mainly attributed to differences in the pre- processing techniques applied to the GRACE

433  solutions used to filter out the high frequencies from the noisy raw data.

434      The importance of this study also resides in the possible applications into which such an

435  interannual ice-sheet total discharge dataset can be involved, as the exploitation in global,

436  regional and coastal ocean modeling. It can be prescribed, in fact, as forcing input in ocean

437  circulation models, in order to study the response of sea level, ocean mass properties and

438  thermohaline circulation to a realistic freshwater coastal discharge. Ocean models, in fact, are

439  a powerful tool for the study of sea level change and for the investigation of the impact that

440  ice-sheet total discharge has, and could have in the future, on the ocean state and in particular

441  on sea level rise. Nevertheless, most of the current OGCMs do not take into account this

442  important source of freshwater input; in fact, due to the lack of time-varying freshwater flux

443  measurements, land runoff and ice discharge used in the current OGCMs simulations only

444  includes climatological estimates that are assumed not to vary inter-annually; therefore ocean

445  simulations cannot take into account increasing ice-sheets contribution and its variability,

446  ignoring, in this way, one of the main cause of global sea level rise.

447   **References.**

448   Adler, R.F., Huffman, G.J., Chang, A., Ferraro, R., Xie, P., Janowiak, J., Rudolf, B.,

449   Schneider, U., Curtis, S., Bolvin, D., Gruber, A., Susskind, J., and Arkin, P.: The Version 2

450   Global Precipitation Climatology Project (GPCP) Monthly Precipitation Analysis (1979-

451   Present). *J. Hydrometeor.*, 4,1147-1167, 2003.

452

453   Alsdorf, D.E., and Lettenmaier, D.P.: Tracking fresh water from space. *Science,* 301, 1491-

454   1494, 2003.

455

456   Brakenridge, G.R., Nghiem, S.V., Anderson, E., and Chien S.: Space-based measurement of

457   river runoff. *Eos, Trans. Amer. Geophys. Union*, 86, 185-188, 2005.

458

459   Bromwich, D., Nicolas, J., and Monaghan, A.: An assessment of precipitation changes over

460   Antarctica and the Southern Ocean since 1989 in contemporary global renalyses. *Journal of*

461   *Climate*, 24, 4189-4209, 2011.

462

463   Dai, A., and Trenberth, K.E.: Estimates of freshwater discharge from continents: latitudinal

464   and seasonal variations. *Journal of hydrometeorology*, 3, 660-687, 2002.

465

466   Dee, D. P., Uppala, S. M., Simmons, A. J., Berrisford, P., Poli, P. et al.: The ERA-Interim

467   reanalysis: configuration and performance of the data assimilation system. *Quarterly Journal*

468   *of the Royal Meteorological Society,* Volume 137, pages 553-597, 2011.

469

470   Enderlin, E.M., Howat, I.M., Jeong, S., Noh, M.J., van  Angelen, J.H., and van den Broeke,

471    M.R.: An improved mass budget for the Greenland ice sheet. *GRL* (41), 866-872, DOI:

472    10.1002/2013GL059010, 2014.

473

474    Ettema, J., van den Broeke, M.R., van Meijgaard, E., van de Berg, W.J., Bamber, J.L., Box,

475    J.E., and Bales, R.C.: Higher surface mass balance of the Greenland ice sheet revealed by

476    high-resolution climate modeling. *Geophys. Res. Lett.*, Vol. 36, L12501,

477    doi:10.1029/2009GL038110, 2009.

478

479    Fekete, B.M., Vörösmarty, C.J., and Grabs, W.: Global composite runoff fields based on

480    observed data and simulated water balance. Global Runoff Data Centre Tech. Rep. 22,

481    Koblenz, Germany, 108 pp, 2000.

482

483    Fekete, B.M., Vörösmarty, C.J., and Grabs, W.: High-resolution fields of global runoff

484    combining observed river discharge and simulated water balances. *Global Biogeochem.*

485    *Cycles*, 16, 1042, doi:10.1029/1999GB001254, 2002.

486

487    Flament, T., and Rémy, F.: Dynamic thinning of Antarctic glaciers from along-track repeat

488    radar altimetry. *Journal of Glaciology* 58(211): 830–840, 2012.

489

490    Frappart, F., and Ramillien, G.: Contribution of GRACE Satellite Gravimetry in Global and

491    Regional Hydrology, and in Ice Sheets Mass Balance. In the book "Water Resources

492    Management and Modeling", edited by Purna Nayak, ISBN 978-953-51-0246-5, InTech,

493    March 3, 2012.

494

495    Frappart, F., Ramillien, G., Maisongrande, P., and Bonnet, M.-P.: Denoising satellite gravity

496    signals by Independent Component Analysis. *IEEE Geosci. Remote Sens. Lett.* 7 421–5, 2010.

497

498    Frappart, F., Ramillien, G., Leblanc, M., Tweed, S.O., Bonnet, M.-P., and Maisongrande, P.:

499    An independent component analysis approach for filtering continental hydrology in the

500    GRACE gravity data. *Remote Sens. Environ.* 115 187–204., 2011.

501

502    Gregory, J.M., and Huybrechts, P.: Ice-sheet contributions to future sea-level change. Philos.

503    Trans. R. Soc. London Ser. A, 364, 1709–1731, 2006.

504

505    Holland, D., Thomas, R.H., De Young, B., Ribergaard, M.H., and Lyberth, B.: Acceleration

506    of Jakobshawn Isbraetriggered by warm subsurface ocean waters. *Nat. Geosc,* 2008.

507

508    IMBIE team: Mass balance of the Antarctic Ice Sheet from 1992 to 2017. Nature 558, 219-

509    222, 2018.

510

511    IPCC: Climate Change 2013: The Physical Science Basis. Contribution of Working Group I

512    to the Fifth Assessment Report of the Intergovernmental Panel on Climate Change [Church,

513    J.A., Clark, P.U., Cazenave, a., Gregory, J.M., Jevrejeva, S., Levermann, A., Merrifield, M.A.,

514    Milne, G.A., Nerem, R.S., Nunn, P.D., Payne, A.J., Pfeffer, W.T., Stammer, D., Unnikrishnan,

515    A.S., (eds.)]. Cambridge University Press, Cambridge, United Kingdom and New York, NY,

516    USA, 2014.

517

518    Ligtenberg, S. R. M., Horwath, M., Van den Broeke, M. R., and Legrésy, B.: Quantifying

519    the seasonal breathing of the Antarctic ice sheet, Geophys. Res. Lett., 39, L23501,

520    doi:10.1029/2012GL053628, 2012.

521

522    Luthcke, S.B., Zwally, H.J., Abdalati, W., Rowlands, D.D., Ray, R.D., et al.: Recent

523    Greenland ice mass loss by drainage system from satellite gravimetry observations.

524    *Sciencexpress* 314:1286-89, doi:10.1126/science.1130776, 2006.

525

526    Marsh, R., Desbruyères, D., Bamber, J. L., De Cuevas, B. A., Coward, A. C., and Aksenov,

527    Y.: Short-term impacts of enhanced Greenland freshwater fluxes in an eddy-permitting ocean

528    model, *Ocean Sci., 6, 749-760,* 2010.

529

530    Mouginot, J., Rignot, E., and Scheuchl, B.: Sustained increase in ice discharge from the

531    Amundsen Sea Embayment, West Antarctica, from 1973 to 2014. *GRL* (41), 1576–1584,

532    DOI:10.1002/2013GL059069, 2013.

533

534    Paulson, A., Zhong, S., and Wahr, J.: Inference of mantle viscosity from GRACE and

535    relative    sea    level    data.    *Geophys.    J.    Int.*    171,    497–508.    doi:    10.1111/j.1365-

536    246X.2007.03556.x, 2007.

537

538    Peltier, W. R.: Global glacial isostasy and the surface of the Ice-Age Earth: The ICE-5G

539    (VM2) model and GRACE. *Annu. Rev. Earth Planet. Sci.*, 32, 111– 149, 2004.

540

541    Ramillien, G., Frappart, F., Güntner, A., Ngo-Duc, T., Cazenave, A., and Laval, K.: Time

542    variations of the regional evapotranspiration rate from Gravity Recovery and Climate

543    Experiment (GRACE) satellite gravimetry. Water Resour. Res., 42, W10403,

544    doi:10.1029/2005WR004331, 2006a.

545

546    Ramillien, G., Lombard, A., Cazenave, A., Ivins, E., Llubes, M., et al.: Interannual

547    variations of ice sheets mass balance from GRACE and sea level. *Glob. Planet. Change*

548    53:198-208, 2006b.

549

550    Rémy, F., Flament, T., Michel, A., and Verron, J.: Ice sheet survey over Antarctica with

551    satellite altimetry: ERS1/2, Envisat, Saral/AltiKa, the key importance of continuous

552    observations along the same repeat orbit. *Int. J. Remote Sens*, 35, 5497–5512, 2014.

553

554    Rémy, F., and Frezzotti, M.: Antarctica ice sheet mass balance. *C. R. Geosci.*, 338, 1084-

555    1097, 2006.

556

557    Rignot, E., Bamber, J.L., Van den Broeke, M.R., Davis, C., Li, Y., et al.: Recent Antarctic

558    ice mass loss from radar interferometry and regional climate modelling. Nat. Geosci. 1:106-

559    10, 2008.

560

561    Rignot, E., Velicogna, I., van den Broeke, M.R., Monaghan, A., and Lenaerts, J.:

562    Acceleration of the contribution of the Greenland and Antarctic ice sheets to sea level rise.

563    Geophys. Res. Lett. 38:L05503. doi:10.1029/2011GL046583, 2011.

564

565    Schmidt, R., Flechtner, F., Reigber, Ch., Schwintzer, P., Günter, A., Doll, P., Ramillien, G.,

566    Cazenave, A., Petrovic, S., Jochman, H., and Wunsch, J.: GRACE observations of changes in

567  continental    water    storage.   *Glob.    Planet.    Change*   50/1–2,    112–126.

568  doi:10.1016/j.gloplacha.2004.11.018, 2006.

569

570  Sheffield, J., Goteti, G., and Wood, E.F.: Development of a 50-yr high-resolution global

571  dataset of meteorological forcings for land surface modeling. *J. Clim.* 19:3088–3111, 2006.

572

573  Shepherd, A., Ivins, E.R., Geruo, A., and Barletta, V.R., et al.: A reconciled estimate of ice-

574  sheet mass balance. *Science* 338(6111): 1183–1189, 2012.

575

576  Simmons, A., Uppala, S., Dee, D., and Kobayashi, S.: ERA-Interim: New ECMWF

577  reanalysis products from 1989 onwards. In Newsletter 110. ECMWF, 2007.

578

579  Stoddart, D.M., et al.: Australia's Antarctic science program. *Department of the*

580  *Environment, Water, Heritage and the Arts, Australian Antarctic Division,* 2008.

581

582  Syed, T.H., Zlotnicki, V., and Rodell, M.: Contemporary estimates of Arctic freshwater

583  discharge   from   GRACE   and   reanalyses.   *Geophys.   Res.   Lett.*,   34,   L19404,

584  doi:10.1029/2007GL031254, 2007.

585

586  Syed, T.H., Famiglietti, J.S., and Chambers, D.P.: GRACE-based estimates of terrestrial

587  freshwater discharge from basin to continental scales. *J Hydrometeorol* 10:22–40, 2009.

588

589  Syed, T. H., Famiglietti, J.S., Chambers, D., Willis, J., Hilburn, K.: Satellite-Based Global

590  Ocean Mass Balance Estimates of Interannual Variability and Emerging Trends in Continental

591    Freshwater Discharge, Proc. Nat. Acad. Sci., 107 (42) 17916-17921; published ahead of print

592    October 4, 2010, doi:10.1073/pnas.1003292107, 2010.

593

594    Tapley, B.D., Bettadpur, S., Watkins, M., and Reigber, C.: The gravity recovery and climate

595    experiment: mission overview and Early results. *Geophys. Res. Lett.* 31, L09607.

596    doi:10.1029/2004GL019920, 2004.

597

598    Undén, P., Rontu, L., Järvinen, H., Lynch, P., Calvo, J., Cats, G., Cuxart, J., Eerola, K.,

599    Fortelius, C., Garcia-Moya, J.A., Jones, C., Lenderlink, G., McDonald, A., McGrath, R.,

600    Navascues, B., Nielsen, N.W., Odergaard, V., Rodrigues, E., Rummukainen, M., Rõõm, R.,

601    Shattler, K., Sass, B.H., Savijärvi, H., Schreur, B.W., Sigg, R., The, H., and Tijm, A.:

602    HIRLAM-5 Scientific Documentation, HIRLAM-5 Project, c/o Per Undén SMHI, S-601 76

603    Norrköping, SWEDEN, 144 p, 2002.

604

605    van den Broeke, M.R., Bamber, J., Lenaerts, J., and Rignot, E.: Ice sheets and sea level:

606    thinking outside the box. *Surv. Geophys*. 32 495–505, 2011.

607

608    van Meijgaard, E., van Ulft, L.H., van de Berg, W.J., Bosveld, F.C., van den Hurk, B.J.J.M.,

609    Lenderink, G., Siebesma, A.P.: The KNMI regional atmospheric climate model RACMO

610    version 2.1. Technical report ; TR – 302, 2008.

611

612    Velicogna, I., and Wahr., J.: Time-variable gravity observations of ice sheet mass balance:

613    Precision and limitations of the GRACE satellite data. Geophysical Research Letters,

614    40(12):3055–3063, 2013. ISSN 1944-8007. doi: 10.1002/grl.50527, 2013.

615

616    Vernon, C. L., Bamber, J. L., Box, J. E., van den Broeke, M. R., Fettweis, X., Hanna, E., and

617    Huybrechts, P.: Surface mass balance model intercomparison for the Greenland ice sheet, The

618    Cryosphere Discuss., 6, 3999–4036, doi:10.5194/tcd-6-3999, 2012.

619

620    Wahr, J., Molenaar, M., and Bryan, F.: Time-variability of the Earth's gravity field:

621    Hydrological and oceanic effects and their possible detection using GRACE. *J. Geophys.*

622    *Res.*, 103, 32,20530,229, 1998.

623

624    Wahr, J., Swenson, S., Zlotnicki, V., and Velicogna, I.: Time-variable gravity from GRACE:

625    First results. *Geophys. Res. Lett.*, 31, L11501, doi:10.1029/2004GL019779, 2004.

626

627    Xie, P., and Arkin, P.A.: Global precipitation: A 17-year monthly analysis based on gauge

628    observations, satellite estimates, and numerical model outputs. *Bull. Amer. Meteor. Soc.*, 78,

629    2539-2558, 1997.

630

631    Zwally, H.J., Li, J., Brenner, A.C., Beckley, M., Cornejo, H.G., Dimarzio, J., Giovinetto,

632    M.B., Neumann, T.A., Robbins, J., Saba, J.L., Yi, D., and Wang, W.: Greenland ice sheet

633    mass balance: distribution of increased mass loss with climate warming: 2003-07 versus

634    1992-2002. *J. Glaciol.*, 57, 1–15, 2011.

**List of figure captions.**

**Figure 1**– Greenland drainage system regions based on surface slopes analyses proposed by Luthcke et al. (2006).

**Figure 2** – Equivalent water height trend over the 2003-2012 period calculated from CSR GRACE solution.

**Figure 3**– Time series of equivalent water height over Greenland (top), East and West Antarctica (middle and bottom, respectively) from the all GRACE solutions. The time series have been computed with respect to 2003-2011 average.

**Figure 4**– Time series of equivalent water height over the 6 drainage basins of Greenland ice-sheet from JPL (top) and GRGS (bottom) solutions. JPL solution has to be intended as representative of the whole ICA-based solutions.

**Figure 5**– Time series of equivalent water height from all the GRACE solutions, over the northern-west (basin 1, top) and the southern-east (basin 4, bottom) drainage basin of Greenland ice-sheet (see Figure 1 for the location of the basin).

**Figure 6**– Time series of equivalent water height from all the GRACE solutions, over the northern-west (basin 1, top) and the southern-east (basin 4, bottom) Greenland drainage basin and the surrounding ocean nearby the coasts.

**Figure 7**– Comparison of Greenland (top panel) and Antarctica (bottom panel) ice discharge estimated from the different methods of total discharge calculation with InSAR observations (magenta line).

**Figure 8**– Monthly climatology (2003-2010) of Greenland (top) and Antarctica (bottom) ensemble-mean total discharge (red lines) and total discharge derived from ice-sheet water

658    mass balance by using different datasets of precipitation.

659    **Figure 9**– Comparison among the different precipitation datasets (2003-2010 climatologies)

660    over Greenland (top) and Antarctica (bottom).

661

662

663

664

665

666

667

668

669

670

671

672

673

674

675

676

677

678
679
680
681
682
683
684
685
686
687
688
689
690
691

692 **Figure 1–** Greenland drainage system regions based on surface slopes analyses proposed by
693 Luthcke et al. (2006).

694
695
696
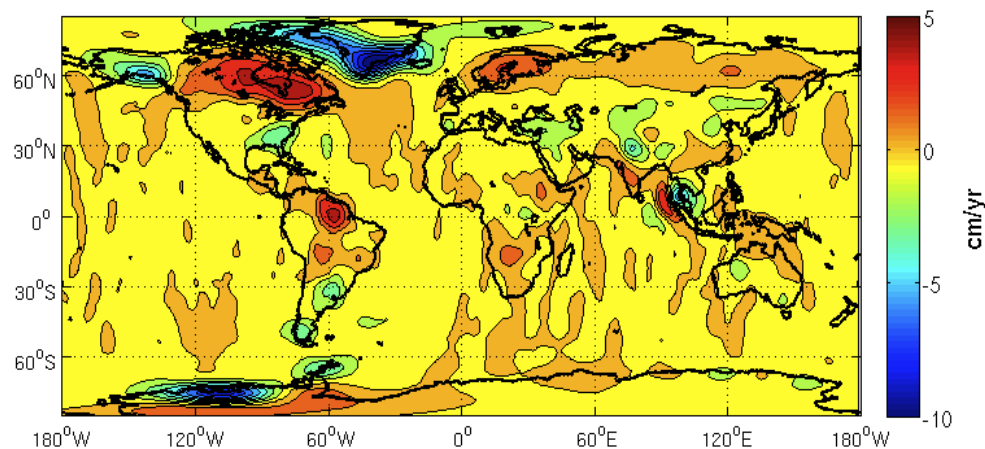
698 **Figure 2 –** Equivalent water height trend over the 2003-2012 period calculated from CSR
699 GRACE solution.
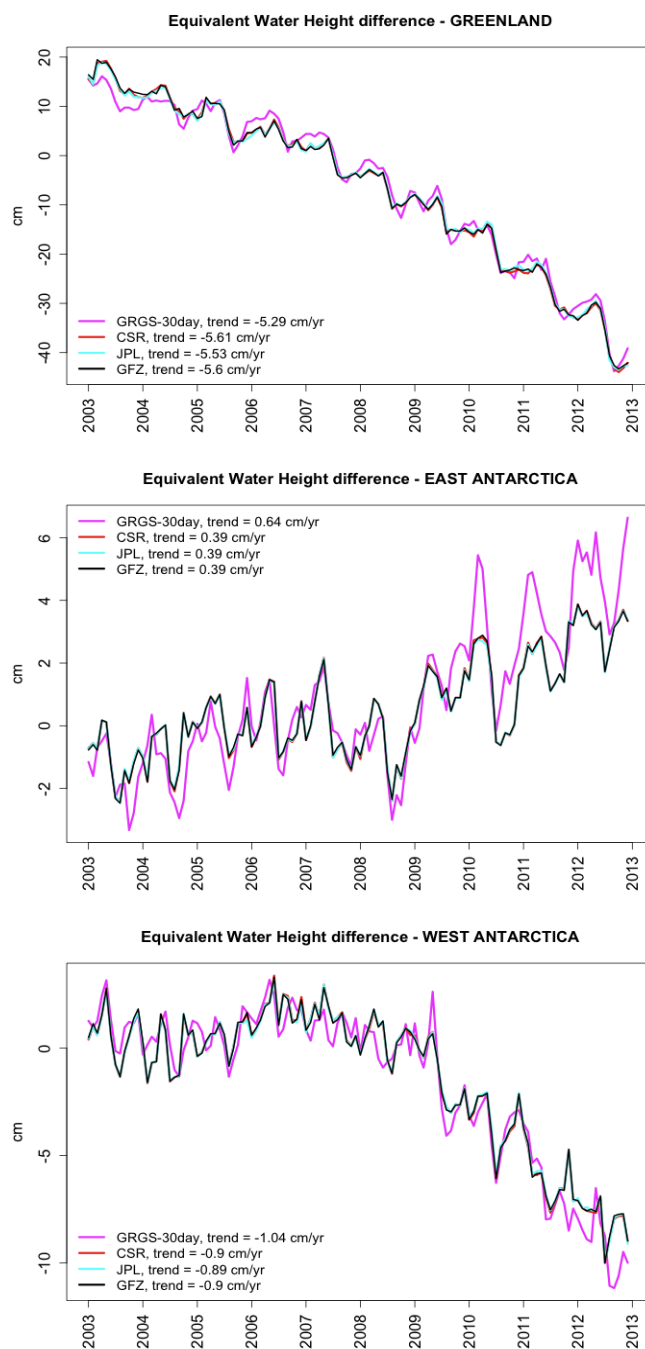
700 **Figure 3–** Time series of equivalent water height over Greenland (top), East and West
701 Antarctica (middle and bottom, respectively) from all GRACE solutions. The time series have

702    been computed with respect to 2003-2011 average.

703

704
705
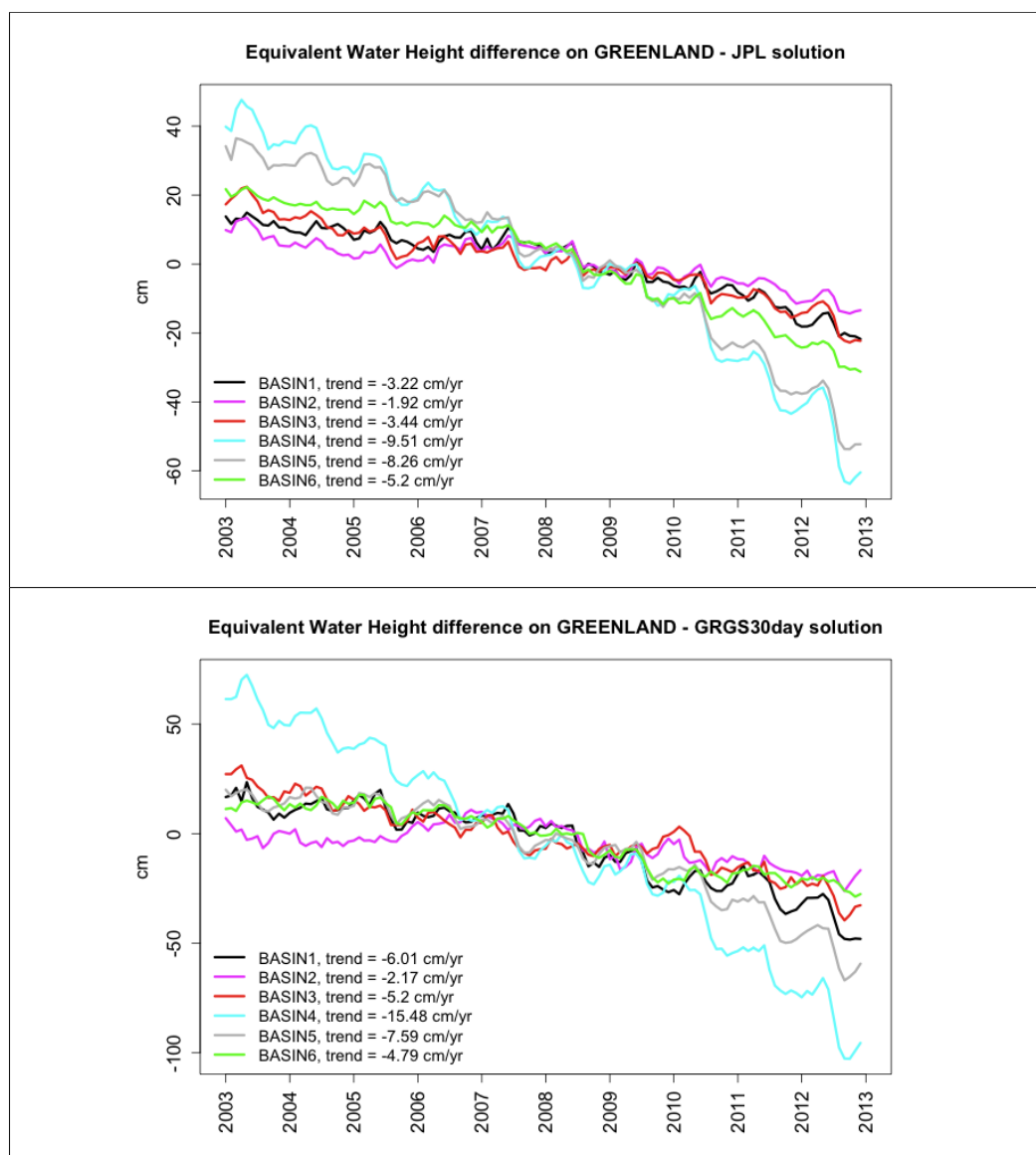
**Figure 4–** Time series of equivalent water height over the 6 drainage basins of Greenland ice-
sheet from JPL (top) and GRGS (bottom) solutions. JPL solution has to be intended as
representative of the whole ICA-based solutions.

710

711

**Figure 5–** Time series of equivalent water height from all the GRACE solutions, over the northern-west (basin 1, top) and the southern-east (basin 4, bottom) drainage basin of Greenland ice-sheet (see Figure 1 for the location of the basin).

715

716

717

718
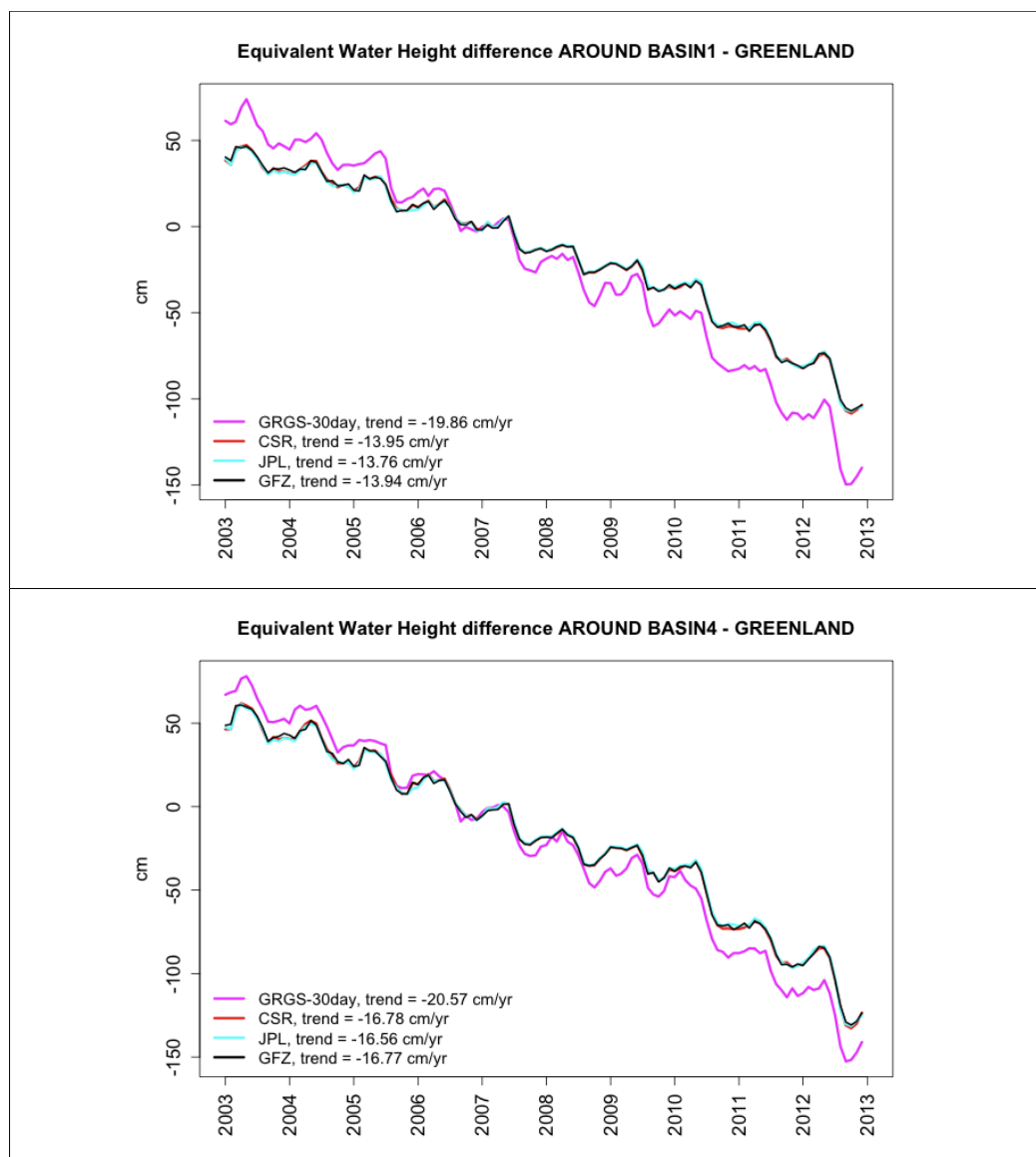
719

**Figure 6**– Time series of equivalent water height from all the GRACE solutions, over the
northern-west (basin 1, top) and the southern-east (basin 4, bottom) Greenland drainage basin
and the surrounding ocean nearby the coast.

723

724

725
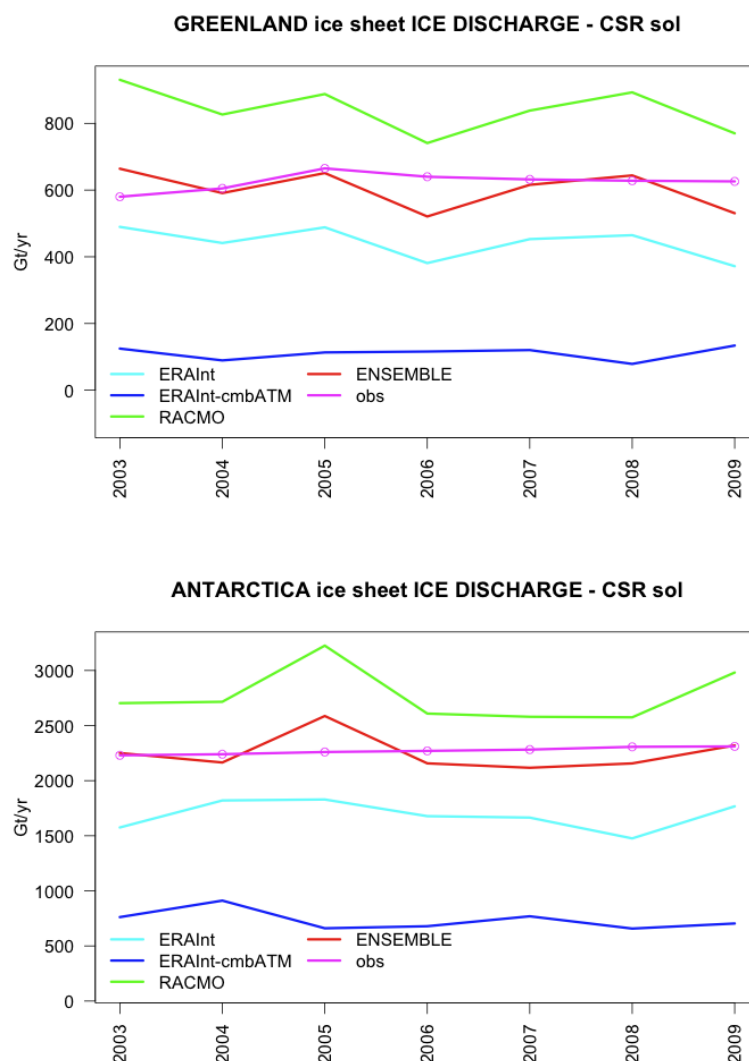
726

**Figure 7**– Comparison of Greenland (top panel) and Antarctica (bottom panel) ice discharge
estimated from the different methods of total discharge calculation with InSAR observations
(magenta line).

730

731

732

733
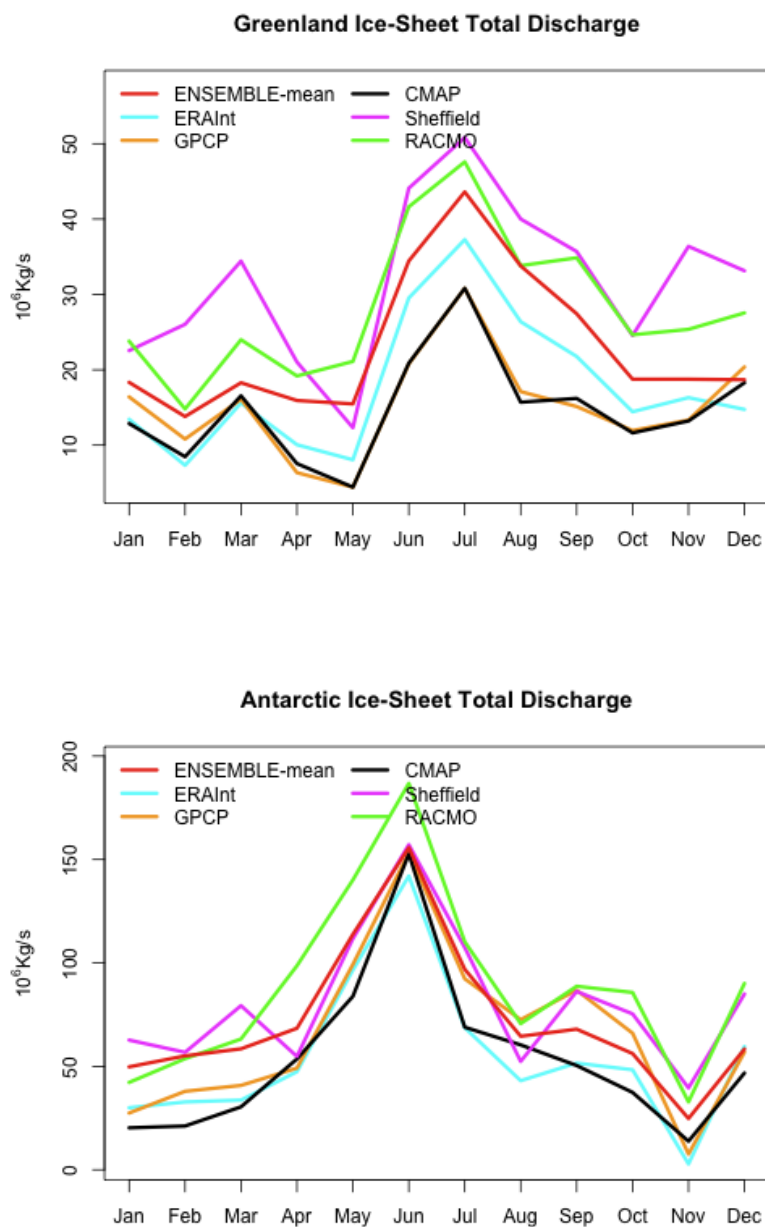
734

735 **Figure 8–** Monthly climatology (2003-2010) of Greenland (top) and Antarctica (bottom)
736 ensemble-mean total discharge (red lines) and total discharge derived from ice-sheet water
737 mass balance by using different datasets of precipitation.

738
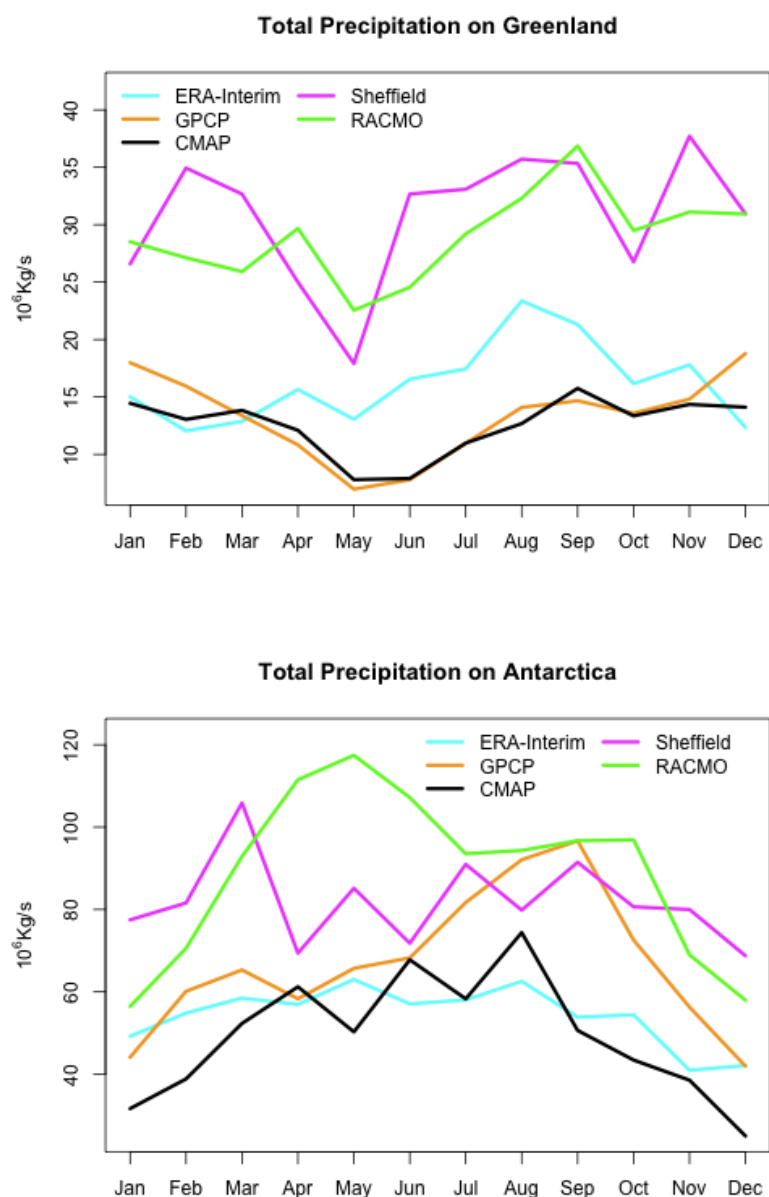
739

740    **Figure 9**– Comparison of different precipitation datasets (2003-2010 climatologies) over
741    Greenland (top) and Antarctica (bottom).